Parton ladder splitting and the rapidity dependence of transverse momentum spectra in deuteron-gold collisions at the BNL Relativistic Heavy Ion Collider

Klaus Werner,[1] Fu-Ming Liu,[2] and Tanguy Pierog[3]
[1]*SUBATECH, Université de Nantes, IN2P3/CNRS, EMN, Nantes, France*
[2]*Central China Normal University, Institute of Particle Physics, Wuhan, China*
[3]*Forschungszentrum Karlsruhe, Institut f. Kernphysik, Karlsruhe, Germany*
(Received 29 June 2005; revised manuscript received 11 May 2006; published 5 October 2006)

We present a phenomenological approach (EPOS), based on the parton model, but going much beyond by incorporating elastic and inelastic parton ladder splitting. Based on this model, we try to understand proton-proton and deuteron-gold (dAu) collisions, in particular the rapidity dependence of transverse momentum results in dAu from all four experiments conducted on the BNL Relativistic Heavy Ion Collider.

DOI: 10.1103/PhysRevC.74.044902 PACS number(s): 25.75.−q, 13.85.Hd, 25.45.−z

I. INTRODUCTION

Interesting new results have been observed in heavy ion collisions at the BNL Relativistic Heavy Ion Collider (RHIC), a large fraction of which are based on transverse momentum spectra. High transverse momenta seem to be suppressed [1,2], but not in the same way for different hadron species [3].

However, any quantitative expression of a suppression or an enhancement needs a reference, and here one usually refers to proton-proton scattering. The first problem, therefore, is to understand sufficiently well proton-proton scattering. This is not trivial. Experimentally, it is difficult to really access the full inelastic cross section; the interaction triggers tend to miss a large fraction of the events. Theoretically, proton-proton scattering is far from being fully understood, in particular concerning particle production at moderate.

A second problem arises due to the fact that unexpected observations in heavy ion collisions provide unnecessary evidence for the formation of a quark-gluon plasma. It may be a phenomenon already present in proton-nucleus scattering. This was the main reason for studying not only gold-gold (AuAu) but also deuteron-gold (dAu) collisions at RHIC [4–8], which produced quite interesting results: the strong high-p_t suppression in AuAu seems to be absent in dAu, so we have clearly a final state effect.

Many features of dAu seem to be qualitatively understood when employing the saturation model [9–12], a recombination model [13], an improved parton model [14–16], and a multiphase model [17]. But what is really missing is a global and quantitative investigation: Can we understand *All* the data presented so far by *All* the experiments, for pp and dAu, in a single approach ? This also gives us the opportunity to cross-check the different experiments, which is not so obvious to do directly.

The purpose of this paper is to present a phenomenological approach (EPOS)—based on the parton model but going much beyond it—and to try to understand p the transverse momentum results in pp and dAu scattering from all four RHIC experiments. All calculations in this paper are based on EPOS version 1.09.

II. IMPROVED PARTON MODEL WITH REMNANTS

The new approach we are going to present is called EPOS, which stands for **E**nergy-conserving quantum mechanical multiple scattering approach, based on **P**artons (parton ladders), **O**ff-shell remnants, and **S**plitting of parton ladders. We will explain the different items in the following discussion; parton ladder splitting will be discussed in a later section.

One may consider the simple parton model to be the basis of hadron-hadron interaction models at high energies. It is well known that the inclusive cross section is given as a convolution of two parton distribution functions with an elementary parton-parton interaction cross section. The latter one is obtained from perturbative QCD; the parton distributions are deduced from deep inelastic scattering. Although these distributions are taken as black boxes, one should not forget that they represent a dynamic process, namely, the successive emission of partons (initial state spacelike cascade), which have to be considered in a complete picture. In addition, the produced partons are generally off-shell, giving rise again to parton emissions (final state timelike cascade). All this is sketched in Fig. 1, in which we also indicate that we refer to this whole structure as a "parton ladder," with a corresponding simple symbol, to simplify further discussion.

Actually our parton ladder is meant to contain two parts [18]: the hard one, as discussed above, and a soft one, which is a purely phenomenological object, parametrized in Regge pole fashion. Several parameters, that determine the parametrization of the soft elementary interaction (soft Pomeron) are essentially fixed to get the pp cross sections right. The pQCD parameters determining the hard ladders (soft virtuality cutoff, K factor, parton emission cutoff, and parton-hadron coupling) are fixed to provide a reasonable parton distribution function (which we calculate, it is not input!).

Still the picture is not complete, since so far we have considered only two interacting partons, one from the projectile and one from the target. These partons leave behind colored projectile and target remnants, so the picture is more complicated than simply projectile/target deceleration.

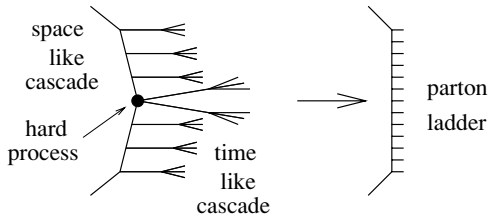

FIG. 1. Elementary parton-parton scattering: the hard scattering in the middle is preceded by parton emissions (initial state spacelike cascade); these partons being usually off-shell, they emit more partons (final state timelike cascade). For all this we use a symbolic parton ladder.

One may simply consider the remnants to be diquarks, providing a string end, but this simple picture seems to be excluded from the strange antibaryon results produced at the CERN super proton synchrotron (SPS) [19].

We therefore adopt the following picture, as indicated in Fig. 2: not only a quark but also a two-fold object takes part directly in the interaction, being a quark-antiquark or a quark-diquark, leaving behind a colorless remnant, which is in general excited (off-shell). So we have finally three white objects: the two off-shell remnants and the parton ladder between the two active partons on either side (by parton we mean quark, antiquark, diquark, or antidiquark). We also refer to "inner contributions" (from parton ladders) and "outer contributions" (from remnants), which reflect the fact that the remnants produce particles mainly at large rapidities and the parton ladders at central rapidities, see Fig. 3. Whereas the outer contributions are essentially energy independent, apart from a shift in rapidity, the inner contributions grows with energy, central rapidities. But at RHIC energies, a substantial remnant contribution remains at midrapidity.

We showed in Ref. [20] that the three-object picture as discussed in this paper can solve the multi-strange baryon problem of Ref. [19].

In practice, a couple of parameters determine remnant properties. We assume the remnants to be off-shell with probability p_O, a mass distribution given as

$$\text{prob} \propto M^{-2\alpha_O}, \tag{1}$$

within the kinematic allowed range of M, with parameter values which are not necessarily the same for nondiffractive and diffractive interactions (the latter ones defined as those without parton ladders). We use currently for p_O 0.75 (dif) and 0.95 (nondif), and for α_O 0.75 (dif) and 1.1 (nondif). Those excitation exponents may give rise to quite high mass remnants; RHIC and SPS data seem to support this. High mass remnants will be treated as strings.

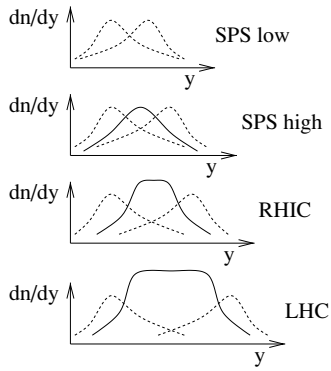

FIG. 3. Inner contributions from the parton ladder (full lines) and outer contributions from the remnants (dashed lines) to the rapidity distribution of hadrons (artist's view). LHC indicates energies reached by the CERN Large Hadron Collider.

Even inclusive measurements often require more information than just inclusive cross sections, for example, via trigger conditions. In any case, for detailed comparisons we need an event generator, which obviously requires information about exclusive cross sections (the widely used pQCD generators are not event generators in this sense, they are generators of inclusive spectra, and a Monte Carlo event is not a physical event). This problem has been known for many years; the solution is Gribov's multiple scattering theory, which has been employed by many authors. This formulation is equivalent to using the eikonal formula to obtain exclusive cross sections from knowledge of the inclusive one.

Recently we indicated inconsistencies in this approach, proposing an "energy-conserving multiple scattering treatment" [18]. The main idea is simple: in the case of multiple scattering, when calculating partial cross sections for double, triple, ... scattering, one has to explicitly account for the fact that the total energy has to be shared among the individual elementary interactions.

A consistent quantum mechanical formulation of multiple scattering requires consideration not only of the (open) parton ladders, discussed so far, but also of closed ladders, representing elastic scattering, see Fig. 4. Closed ladders do not contribute to particle production, but they are crucial since they affect substantially the calculations of partial cross

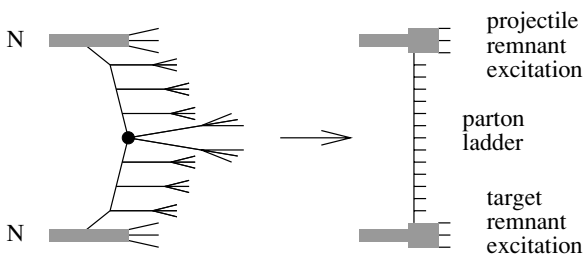

FIG. 2. Complete picture, including remnants, which are an important source of particle production at RHIC energies.

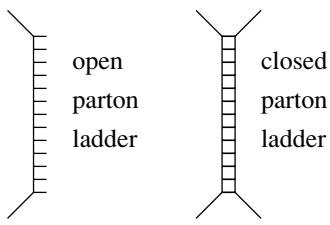

FIG. 4. Two elements of the multiple scattering theory: open ladders, representing inelastic interactions, and closed ladders, representing elastic interactions.

sections. Actually, closed ladders simply lead to large numbers of interfering contributions for the same final state, all of which have to be summed up to obtain the corresponding partial cross sections. This multiple scattering approach, described in detail in [18], allows us to compute partial cross sections, as, for example, the cross section of having n parallel ladders involved, with ladder end light cone momentum fractions $x_1^+, x_1^-, \ldots, x_n^+, x_n^-$, and the corresponding transverse momenta $\vec{p}_{t1}{}^+, \vec{p}_{t1}{}^-, \ldots, \vec{p}_{tn}{}^+, \vec{p}_{tn}{}^-$ ("+" and "−" refer to, respectively, projectile and target side). It is a unique feature of our approach to consider explicitly energy-momentum sharing at this level (the "E" in the name EPOS). We can do the complicated calculations of partial cross sections, since we fit the result of a numerical calculation of a squared amplitude corresponding to a (open) parton ladder of energy $\sqrt{s}$, using a simple form αs^β, which allows us then to perform analytical calculations.

The partial cross sections are formulated in impact parameter (b) space, real cross sections (in mb) are obtained after b integration. These partial cross sections can be interpreted as probability distributions, enabling us to use Monte Carlo techniques. Since we are dealing with multidimensional probability distributions, we have to employ very sophisticated Markov chain techniques to generate configurations.

Computing partial cross sections and generating the corresponding configurations are only half the story. Suppose we have a double scattering (two ladders) in pp scattering, with ladder end momenta obtained as described above. How do we obtain the corresponding partons which "make" the ladders, and how do we finally obtain the hadrons?

Let us first discuss the generation of partons. This is based on exactly the same formulas used to compute partial cross sections, since all these formulas may serve as probability distributions [18]. We obtain not only the probabilities for soft versus hard scattering, but also the probability distribution for parton generation in the case of hard scattering. Using the same formulas for partial cross sections and parton generation is again a unique feature of our approach. In other models, energy sharing is only considered in the case of particle production, not for partial cross sections.

Finally, we have to deal with the difficult question of how these partons will be transformed into observable hadrons. Lacking a fundamental understanding, we content ourselves with a simple parametrization of hadron production, employing the relativistic string model. It is believed that the successive parton emission procedure provides finally a longitudinal (one-dimensional) color field, and the relativistic string is the most simple one-dimensional covariant object. String fragmentation uses just some highly plausible symmetry arguments, all the unknown details are hidden in a few simple parameters. Technically, the procedure consists of two steps: given the partons, strings are formed; then, these strings "fragment" into hadrons. In the following, we sketch the main ideas, for details see Ref. [18].

A string is a two-dimensional surface $x(\sigma, \tau)$ in Minkowski space. Postulating a simple (Nambu-Goto) action, one obtains a simple wave equation, and the string $x(\sigma, \tau)$ can be expressed completely in terms of its initial velocity $g(\sigma) = \partial x/\partial\tau(\sigma, \tau = 0)$. Here, we consider only strings with a piecewise constant function g, which are called kinky strings. So the string is characterized by a sequence of σ intervals $[\sigma_k, \sigma_{k+1}]$ and the corresponding constant values (say v_k) of g in these intervals. Such an interval with the corresponding constant value of g is referred to as a kink.

Now we are in a position to map partons onto strings. A parton ladder may be identified with sequences of partons of the type $q - g - g - \ldots - g - \bar{q}$, with soft "end partons" q and $\bar{q}$, and hard inner gluons g. The mapping is done in the following way: we identify such a sequence with a kinky string by requiring "parton = kink", which means that we identify the partons of the above sequence with the kinks of a kinky string, such that the lengths of the σ intervals are given by the parton energies, and the kink velocities are just the parton velocities. As discussed earlier, the string evolution is then completely given by these initial conditions [18], expressed in terms of parton momenta.

Hadron production is finally realized via string breaking, such that string fragments are identified with hadrons. Here, we employ the so-called area law hypothesis: the string breaks within an infinitesimal area dA on its surface with a probability proportional to this area, $dP = p_B dA$, where p_B is the fundamental parameter of the procedure. An elegant realization is employed, in which we make use of the particular dynamics of strings with piecewise constant initial conditions [18].

Although longitudinal momenta are much more important than transverse ones, the latter cannot be ignored. Suggested by the uncertainty principle, a transverse momentum is generated at each breaking, which means that four-vectors p_t and $-p_t$ are assigned to the string ends at both sides of the break point. We choose the absolute value $k = |\vec{p}_t|$ of the transverse momentum according to the distribution $f(k) \propto \exp(-k/2\bar{p}_t)$, with a parameter $\bar{p}_t$.

A string as a whole has some flavor, carried by the partons at its two extremities. Additional flavor is created at each break point in the form of a quark-antiquark or a diquark-antidiquark pair of a certain flavor. The corresponding probabilities are $1 - p_D$ and p_D, the latter being a free parameter of the model. We introduce a parameter p_S, which gives the relative weight of u to d to s flavor production as $1 : 1 : p_S$.

Having determined the break points and the associated flavors, we can easily compute the four-momenta (and thus the masses) and flavors of the string segments, which we identify with corresponding hadrons or resonances.

As discussed above, there are four important fragmentation parameters: the break probability (per unit space-time area) p_B, which determines whether a string breaks earlier or later; the diquark break probability p_D; the strange break probability p_S; and the mean transverse momentum $\bar{p}_t$ of a break, with obvious consequences for baryon and strangeness production, and the p_t of the produced hadrons. We use three sets of these parameters for the three types of strings: soft, kinky (hard) and, remnant strings. We do not really use the full freedom of these parameters, but one single set would not work if we are interested in high precision. Surprisingly p_S is 0.14 for soft and 0.06 for kinky and remnant strings. Maybe this reflects the fact that soft strings may have low masses, where strangeness is suppressed, and which needs some compensation. The parameter p_D is 0.06 for soft and remnant strings and 0.09

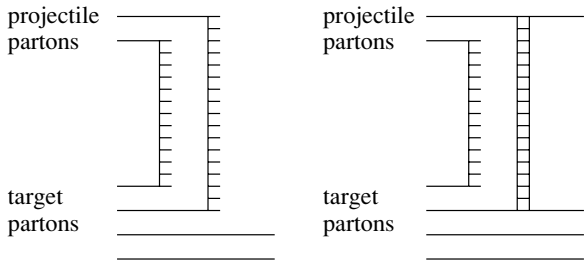

FIG. 5. Basic parton-parton interaction in nucleus-nucleus collisions: a projectile parton always interacts with exactly one parton on the other side either elastically (closed parton ladder) or inelastically (open parton ladder).

for kinky strings. For p_B, we use 0.53 (soft), 0.30 (kinky), and 0.77 (remnant).

III. SPLITTING OF PARTON LADDERS

Let us first consider very asymmetric nucleus-nucleus collisions, such as proton-nucleus or deuteron-nucleus. The formalism developed earlier for pp can be generalized to these nuclear collisions, as long as one assumes that a projectile parton always interacts with exactly one parton on the other side, elastically or inelastically (realized via closed or open parton ladders), see Fig. 5. We employ the same techniques as those developed in the previous section. The calculations are complicated and require sophisticated numerical techniques, but they can be done. The corresponding results for dAu will be discussed later.

In the case of protons (or deuterons) colliding with heavy nuclei (such as gold), there is a complication that has to be taken into account. Suppose an inelastic interaction involves an open parton ladder, between a projectile and some target parton. The fact that these two partons interact implies that they are close in impact parameter (transverse coordinate). Since we have a heavy target, many target partons are available, and there is a good chance of finding one among them being close in impact parameter to the two interacting partons. In this case, it may be quite probable that a parton from the ladder interacts with this second target parton, inelastically or elastically, as shown in Fig. 6.

As mentioned earlier, "ladder" is a symbolic notation, covering soft contributions as well as "real" perturbative parton ladders. Even the latter ones are in general coupled to projectile and target via soft pieces [18]. In the case of soft ones, we still talk about partons, but they are nonperturbative partons. We expect that ladder splitting occurs more likely in the soft regions, and that the parallel legs after the splitting are more likely soft.

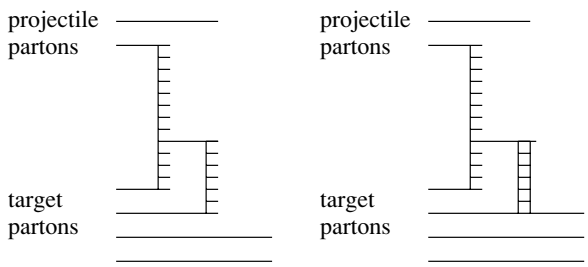

FIG. 6. Inelastic and elastic "rescattering" of a parton from the parton ladder with a second target parton. We talk about (inelastic and elastic) splitting of a parton ladder.

Let us first discuss the effects of elastic splitting. The squared amplitude for an elementary inelastic interaction involving two partons with light cone momentum shares $x^+ = 2p^+/\sqrt{s}$ and $x^- = 2p^-/\sqrt{s}$ can be parametrized quite accurately as [18]

$$\alpha\,(x^+)^\beta (x^-)^\beta, \tag{2}$$

with two parameters α and β depending on the squared energy s and the impact parameter b ($\sqrt{s}$ is the proton-proton c.m. system energy). Any addition of an elastic contribution (closed ladder), be it in parallel or via splitting, provides an interference term, which contributes negatively to (partial) cross sections. So an additional elastic leg, even though it does not affect particle production, provides screening. Model calculations show that adding elastic splittings to the basic diagrams modifies the corresponding squared amplitude as

$$\alpha\,(x^+)^\beta (x^-)^{\beta+\varepsilon}, \tag{3}$$

and therefore the whole effect can be summarized by a simple positive exponent ε, which suppresses small light cone momenta. So the existence of many target partons effectively screens small x contributions, which agrees qualitatively with the concept of saturation. But this is only part of the whole story; several other aspects have to be considered.

An additional effect is the transport of transverse momentum via an attached closed ladder, as shown in Fig. 7. Such a transport we use already in the basic parton model, when it comes to diffractive scattering, realized via a closed ladder. Here, some transverse momentum transfer is needed to explain the transverse momentum spectra of protons at large x (in the diffractive region). In the case of diffractive target excitation, the projectile gets simply a p_t kick. We should have the same phenomenon in the case of elastic splitting: the ladder parton involved in the interaction should get a p_t kick in the ame way as the proton in diffractive scattering.

Let us turn to inelastic splitting, Fig. 8. Consider the example shown in the figure. The upper part has only an ordinary parton ladder, so we expect normal hadronization. However, the lower part has two parallel ladders which are

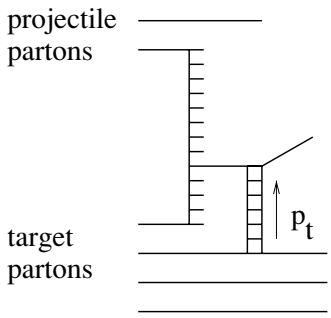

FIG. 7. Transport of transverse momentum via an attached closed ladder.

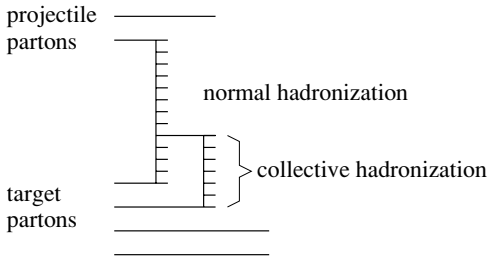

FIG. 8. Hadron production in the case of inelastic ladder splitting.

also close in space, since they have a common upper end and the lower ends are partons close in impact parameter, so the hadronization of the two ladders is certainly not independent. Therefore, we expect some kind of collective hadronization of two interacting ladders. Here, we only considered the most simple situation; one may also imagine three or more close ladders, hadronizing collectively.

If we allow ladders to split, then perhaps they could merge again and form loops. In fact, they can; only we do not need to treat this explicitly, since the splitting concerns mainly the soft ladders (or pieces), and these soft ladders are treated in an effective, phenomenological way via parametrization. So we can easily absorb loops into our effective soft ladders. This cannot be done with the splitting, since the external legs may be attached to different nuclei.

So far, we have discussed in a qualitative fashion the consequences of elastic and inelastic parton ladder splitting. The strength of the effects will certainly depend on the target mass, via the number Z of partons available for additional legs. The number Z of available partons will also increase with energy, so at high enough energy the abovementioned effects can already happen in pp collisions.

IV. REALIZATION OF LADDER SPLITTING EFFECTS

The basic quantity for a numerical treatment of the ladder splitting effects is the number Z of partons available for additional legs; more precisely, we have Z_T for counting legs on the target side and Z_P for counting legs on the projectile side. Let us treat Z_T (corresponding discussion for Z_P). Consider a parton in the projectile nucleon i which interacts with a parton in target nucleon j. The number $Z_T(i, j)$ of additional legs has two contributions, one counting the legs attached to the same nucleon j, and one counting the legs attached to the other nucleons $j' \neq j$. We assume the form

$$Z_T(i, j) = z_0 \exp\bigl(-b_{ij}^2/2b_0^2\bigr) + \sum_{\substack{\text{target nucleons} \\ j' \neq j}} z_0' \exp\bigl(-b_{ij'}^2/2b_0^2\bigr), \tag{4}$$

where b_{ij} is the distance in impact parameter between i and j. The coefficients z_0 and z_0' depend logarithmically on the energy, as

$$z_0 = w_Z \log s/s_M, \tag{5}$$

$$z_0' = w_Z \sqrt{(\log s/s_M)^2 + {w_M}^2}, \tag{6}$$

$[\log(x) := \max(0, \ln(x))]$ and the impact parameter width is $b_0 = w_B \sqrt{\sigma_{\text{inel}pp}/\pi}$, with parameters w_B, w_Z, w_M, and s_M. We then define

$$Z_T(j) = \sum_i Z_T(i, j). \tag{7}$$

We suppose that all the effects of the parton ladder splitting can be treated effectively, meaning that the correct explicit treatment of splittings is equivalent to the simplified treatment without splittings, but with certain parameters modified, expressed in terms of Z. We do this is not only to simplify our life. Even an explicit dynamic treatment remains a phenomenological approach with many uncertainties about the splitting vertices. So we prefer to have simple parametrizations rather than a very complicated but uncertain dynamic treatment.

So which quantities depend on Z, and how? In the following, the symbols a_i are constants, used as fit parameters. The elastic splitting leads to screening, which is expressed by the screening exponents $\varepsilon = \varepsilon_S$ (for soft ladders) and $\varepsilon = \varepsilon_H$ (for hard ladders), and here we assume

$$\varepsilon_S = a_S \beta_S Z, \tag{8}$$

$$\varepsilon_H = a_H \beta_H Z, \tag{9}$$

where β_S and β_H are the usual exponents describing soft and hard amplitudes. Concerning the transport of transverse momentum, we suppose

$$\Delta p_t = a_T p_0 n_q Z, \tag{10}$$

where n_q is the number of quarks of the objects in the hadronization process (1 for quarks, 2 for diquarks), and $p_0 = 0.5$ GeV is just used to define a scale.

Let us now address collective hadronization. We will actually "absorb" the multiple ladders into the remnants, which are usually treated as strings. Now we treat them as strings with modified string break parameters to account for collective hadronization. We modify the break probability (per unit space-time area) p_B, which determines whether a string breaks earlier or later, the diquark break probability p_D, the strange break probability p_S, and the mean transverse momentum $\bar{p}_t$ of a break, as

$$p_B \to p_B - a_B Z, \tag{11}$$

$$p_D \to p_D (1 + a_D Z), \tag{12}$$

$$p_S \to p_S (1 + a_S Z), \tag{13}$$

$$\bar{p}_t \to \bar{p}_t (1 + a_P Z), \tag{14}$$

with positive parameters a_i. So with increasing Z, a reduced p_B will lead to more particle production; an increased p_D, p_S, and $\bar{p}_t$ will lead to more baryon-antibaryon production, more strangeness production, and an increased p_t for each string break.

The parameters s_M, w_i, and a_i are chosen to reproduce the RHIC pp and dAu data shown in this paper, as well as p_t spectra for identified pions, kaons, and protons [21]. We

TABLE I. Best fit values for splitting parameters. Included in the fit are data not shown in this paper.

Coefficient	Corresponding variable	Value
s_M	Minimum squared screening energy	$(25\ \mathrm{GeV})^2$
w_M	Defines minimum for z_0'	6.000
w_Z	Global Z coefficient	0.080
w_B	Impact parameter width coefficient	1.160
a_S	Soft screening exponent	2.000
a_H	Hard screening exponent	1.000
a_T	Transverse momentum transport	0.025
a_B	Break parameter	0.070
a_D	Diquark break probability	0.110
a_S	Strange break probability	0.140
a_P	Average break transverse momentum	0.150

also compare the experimental energy dependence of cross sections [22], hadron multiplicities [23], and (pseudo)rapidity distributions [24,25] in pp or $p\bar{p}$. The best fit parameters are shown in Table I.

V. RESULTS FOR PROTON-PROTON

Ladder splitting is quite important for pp at very high energies, where cross sections and multiplicities are considerably suppressed because of screening. At RHIC energies, however, the effects are small: the total cross section is reduced by 5%, the multiplicity by 10%. Concerning the transverse momentum spectra to be discussed in detail in the following, the effect is hardly visible.

When comparing charged particle p_t spectra in pp from the different RHIC experiments, one has to keep in mind that STAR collaboration refers to non-single-diffractive (NSD) events rather than inelastic ones. To demonstrate the difference between the two, we show in Fig. 9 the UA5 [26] Collaboration pseudorapidity distributions for NSD and inelastic events, together with EPOS simulations. For the simulation of NSD events, we use simply the same requirement as used in the experiment (coincidence of charged particles in a forward and backward pseudorapidity interval).

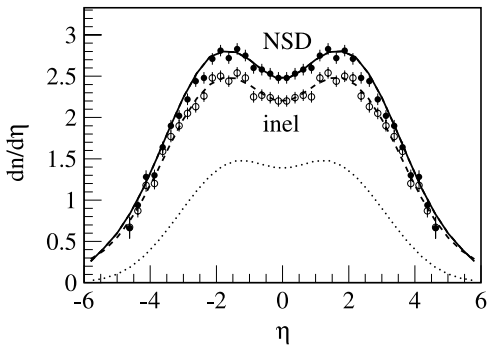

FIG. 9. Pseudorapidity distribution for inelastic and NSD events in $p\bar{p}$ collisions at 200 GeV. Lines are EPOS results; the points are data [26]. Dotted line represents the inner contribution to the inelastic distribution (many particles are coming from remnants).

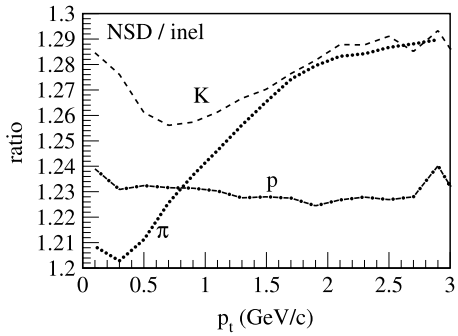

FIG. 10. Ratio of $\mathrm{NSD}^{\mathrm{BBC}}$ differential yield to inelastic differential yield, in pp collisions, for pions (π), kaons (K), and protons (p).

In the case of STAR, one could also define NSD as the events accepted by the beam beam counter (BBC). What is actually done is somewhat different. The differential cross section according to BBC is multiplied by 30/26, in order to correspond to what Pythia defines to be non-single-diffractive, corresponding to 30 mb. Then, again based on Pythia, it is argued that the inelastic differential yield for inelastic events is obtained essentially (with a small correction at small p_t) by multiplying by 30/42 (just the ratio of the cross sections), since single-diffractive (SD) events do not contribute to particle production. So, the originally measured differential yield and the inelastic one differ essentially by a factor of 42/30 = 1.4. This is not quite what EPOS calculations provide when simulating NSD events with the BBC trigger condition and comparing with inelastic events. As seen in Fig. 10, the ratio of the $\mathrm{NSD}^{\mathrm{BBC}}$ differential yield to the inelastic differential yield, rather than being 1.4, differs considerably as a function of p_t and also depends on the particle species.

In Fig. 11, we show p_t spectra (differential yields) for NSD events, compared to STAR data [27], and for inelastic events, compared to PHENIX data [6,28]. Simulation and data agree within 15% (over 6 orders of magnitude).

When studying (later) dAu collisions, there will be plenty of discussion concerning the pseudorapidity dependence of certain effects. It is therefore necessary to first check the pseudorapidity dependence of p_t spectra for pp.

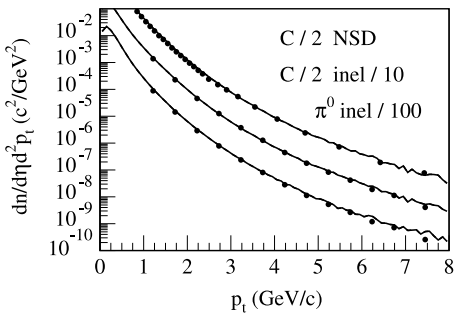

FIG. 11. Differential yields in pp collisions as a function of p_t for (from top to bottom) charged particles (over 2) for NSD events, charged particles (over 2) for inelastic events, and neutral pions for inelastic events. Lines are EPOS simulations; points are data from STAR [27] and PHENIX [6,28]. The two agree within 15% (over six orders of magnitude).

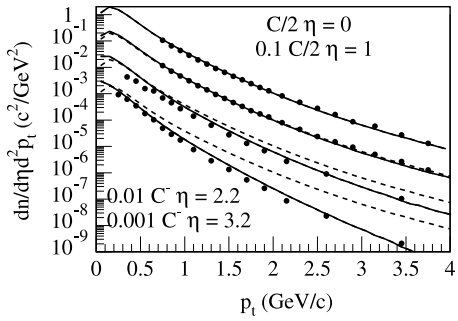

FIG. 12. Inelastic differential yields in *pp* collisions as a function of p_t for (from top to bottom) charged particles (over 2) at $\eta = 0$ and $\eta = 1$; negative particles at $\eta = 2.2$ and $\eta = 3.2$ (always displaced by factors of 10). Lines are EPOS simulations; points are data [7]. We also plot (dashed) the simulation curve at $\eta = 0$, multiplied by 0.1, 0.01, and 0.001, to serve as reference.

In Fig. 12, we plot inelastic differential yields as a function of p_t, at different pseudorapidities; $\eta = 0$, $\eta = 1$, $\eta = 2.2$, and $\eta = 3.2$. We show EPOS simulations compared to BRAHMS data [7]. We also plot (dashed line) the simulation curve at $\eta = 0$, multiplied by 0.1, 0.01, and 0.001, to have a reference for the results at the other pseudorapidities. The spectra clearly get softer with increasing η.

VI. RESULTS FOR DEUTERON-GOLD

All screening effects are linear in Z, so it is worthwhile to first investigate Z. In very asymmetric collisions such as dAu, the projectile Z is essentially zero, whereas the target Z differs considerably from zero. As shown in Fig. 13 (and obvious from the definition), Z_T increases linearly with the number of collisions. So Z is essentially a centrality measure. In Fig. 14, we show the Z distribution for the different centrality classes. In this way, one understands easily how the different centrality classes are affected by the splitting effects.

In the following, we define centrality via the impact parameter variable. A more correct definition (when comparing with experiments) via multiplicities in given rapidity intervals has been tested and gives the same results.

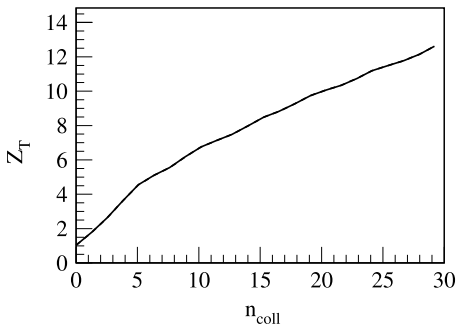

FIG. 13. Target Z as a function of centrality, expressed in terms of the number of binary collisions, for dAu.

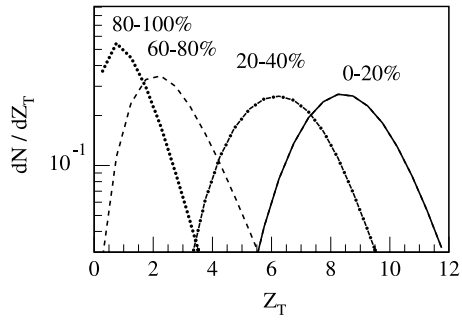

FIG. 14. Z distribution for different centrality classes.

Although we are mainly interested here in transverse momentum spectra, we still show first of all the pseudorapidity spectra, which finally determine the normalization of the p_t spectra. In Fig. 15, we show pseudorapidity spectra in minimum bias dAu collisions: EPOS simulations, compared to data from PHOBOS [29], STAR [4], and BRAHMS [30]. We also show different contributions to the simulated distribution. We distinguish inner and outer (projectile and target) contributions, where the outer contributions are meant to contain the multiple ladders, originating from ladder splittings, treated in a collective way, as discussed above. The inner contribution comes from ordinary ladders in the middle. The asymmetry of the distribution is clearly due to the target remnant contribution (the projectile contribution, not shown, is very small). In Figs. 16 and 17, we show pseudorapidity spectra for central and peripheral dAu collisions.

Let us now turn to p_t spectra. One of the first observations concerning p_t spectra in dAu collisions was the fact that not only does the nuclear modification factor show a nontrivial behavior, but also this behavior seems to be strongly pseudorapidity dependent, even when varying η by only one unit. We will investigate this question in the following discussion.

In Fig. 18, we show transverse momentum spectra of charged particles in dAu collisions at different centralities and at different pseudorapidities. The four figures represent minimum bias, central (0%–20%), mid-central (20%–40%), and peripheral (40%–100%) collisions. For each figure, spectra for four pseudorapidity intervals are

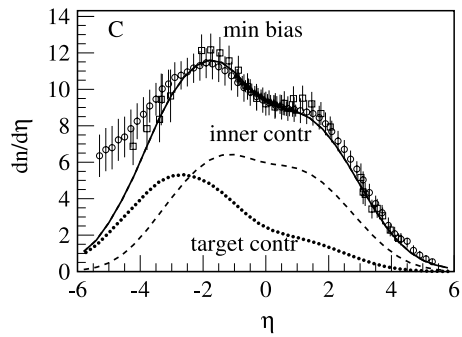

FIG. 15. Pseudorapidity spectra of charged particles in minimum bias dAu collisions. Lines are EPOS simulations; points are data from PHOBOS [29] (circles), STAR [4] (triangles), BRAHMS [30] (squares). We also show the inner and outer target contributions to the simulated distribution.

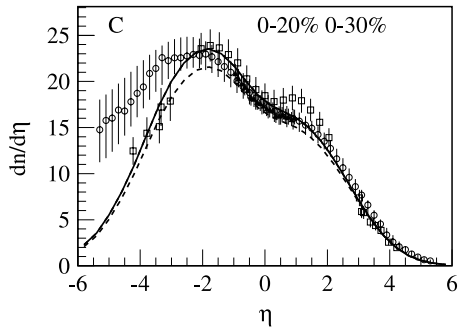

FIG. 16. Pseudorapidity spectra of charged particles for central dAu collisions. Solid lines are EPOS simulations for 0%–20%; dashed lines, for 0%–30%. Points are data from PHOBOS [31] (0%–20%, circles), STAR [4] (0%–20%, triangles), BRAHMS [30] (0%–30%, squares).

shown: $[-1, -0.5]$, $[-0.5, 0]$, $[0, 0.5]$, and $[0.5, 1]$. We simply refer to the corresponding mean values, $\eta = -0.75$, $\eta = -0.25$, $\eta = 0.25$, and $\eta = 0.75$. For better visibility, the different curves have been displaced by factors of 10. Solid lines are EPOS simulations, points are data [4], both agree within 10%–20%. Although looking directly at spectra does not really allow us to see systematic differences between the different curves, it is still useful to first check that the absolute curves agree, before investigating ratios.

To observe any anomalous behavior, one usually plots ratios, such as the nuclear modification factor (ratio R_{AA} of the nucleus-nucleus spectrum to the proton-proton result, divided by the number of binary collisions). The disadvantage is that the corresponding pp spectrum has to be known, with a sufficient precision. An alternative procedure is the use of ratios $R_{\rm cp}$ of central to peripheral results, each divided by the coresponding number of binary collisions. In Fig. 19, we show the $R_{\rm cp}$ ratios at the four pseudorapidities used before. Here, central refers to 0%–20% and peripheral to 40–100%. We also show the corresponding EPOS results, with parton ladder splitting turned off. These curves are cut off at $p_t = 3$ GeV/c, to avoid the strong statistical fluctuations that spoil the figure.

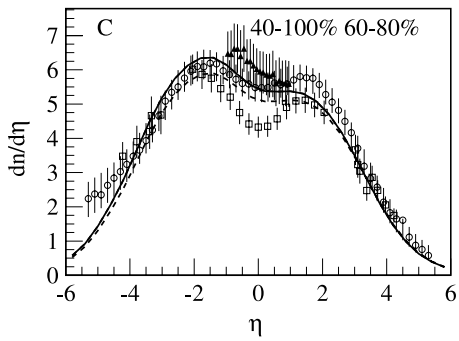

FIG. 17. Pseudorapidity spectra of charged particles for peripheral dAu collisions. Solid lines are EPOS simulations for 40%–100%; dashed lines, for 60%–80%. Points are data from PHOBOS [31] (60%–80%, circles), STAR [4] (40%–100%, triangles), BRAHMS [30] (60%–80%, squares).

The no-parton-ladder-splitting curve stays well below 1 in the shown range. It will finally reach 1 at large p_t. The full EPOS simulations show quite a different behavior; $R_{\rm cp}$ increases strongly between 1 and 2 GeV/c, to stay constant (or decrease) beyond. The statistical fluctuations do not really allow very precise predictions beyond 4 GeV/c. The strong increase between 1 and 2 GeV/c is due to collective hadronization on the target side, which leads to an increased transverse momentum production. As seen is Fig. 15, target-side hadronization extends even to forward pseudorapidities, so it is quite visible in the whole η range $[-1,1]$. The effect is simply somewhat stronger at backward compared to forward rapidity, since target hadronization contributes more. But the difference is not very big. The increase of $R_{\rm cp}$ with p_t is partly also due to the momentum transfer from the elastic splitting, which should affect equally backward and forward pseudorapidities. The variation of the shape of $R_{\rm cp}$ with pseudorapidity is quite small; the main modification is actually an overall factor due to the fact that the particle density increases toward smaller pseudorapidities, as seen from Fig. 15.

A direct way to investigate the pseudorapidity dependence of spectra is provided by the ratio of spectra at backward to forward pseudorapidities, like $\eta = -0.75/\eta = 0.75$, as shown in Fig. 20. Here, one observes a slight increase between 0 and 2 GeV/c. This means that the $R_{\rm cp}$ at backward pseudorapidity increases a bit more than the one at forward pseudorapidity, which we understand since there is somewhat more target side collective hadronization at backward pseudorapidity.

We now consider an even larger pseudorapidity variation: we investigate how the nuclear modification factors vary in the pseudorapidity range 0 to 3.2. Before comparing them to data, we show the results of full EPOS simulations, as well as those with parton ladder splitting turned off. In Fig. 21, we show the nuclear modification factors for charged particles in minimum bias dAu collisions at different pseudorapidities. Whereas the no-splitting curves hardly change with p_t and decrease with pseudorapidity, the full calculations show, of course, the same decrease with pseudorapidity; but all curves increase substantially with p_t between 1 and 3 GeV/c. This confirms the observation made earlier by studying the variation in the η range -1 to 1.

In the following, we will compare the simulations with data from all four RHIC experiments. In Fig. 22, we collect all published data on charged particle nuclear modification factors in minimum bias dAu collisions at (or close to) $\eta = 0$, together with the corresponding simulations. We show minimum bias results at $\eta = 0$ from STAR [5], at $\eta = 0.4$ from PHOBOS [8], 0%–88% centrality results at $\eta = 0$ from PHENIX [6], and minimum bias data at $\eta = 0$ from BRAHMS [7]. We also show minimum bias EPOS simulations at $\eta = 0$ and $\eta = 0.4$, not feed-down corrected minimum bias simulations, and 0%–88% centrality results at $\eta = 0$. We first of all observe that the different simulation results are quite close to each other; so changing slightly the pseudorapidity, using the centrality definition, or making feed down corrections does not affect the final result too much. The variation in the experimental data is much larger. On the upper end, we have the STAR data; but based on the above discussion on pp results, we

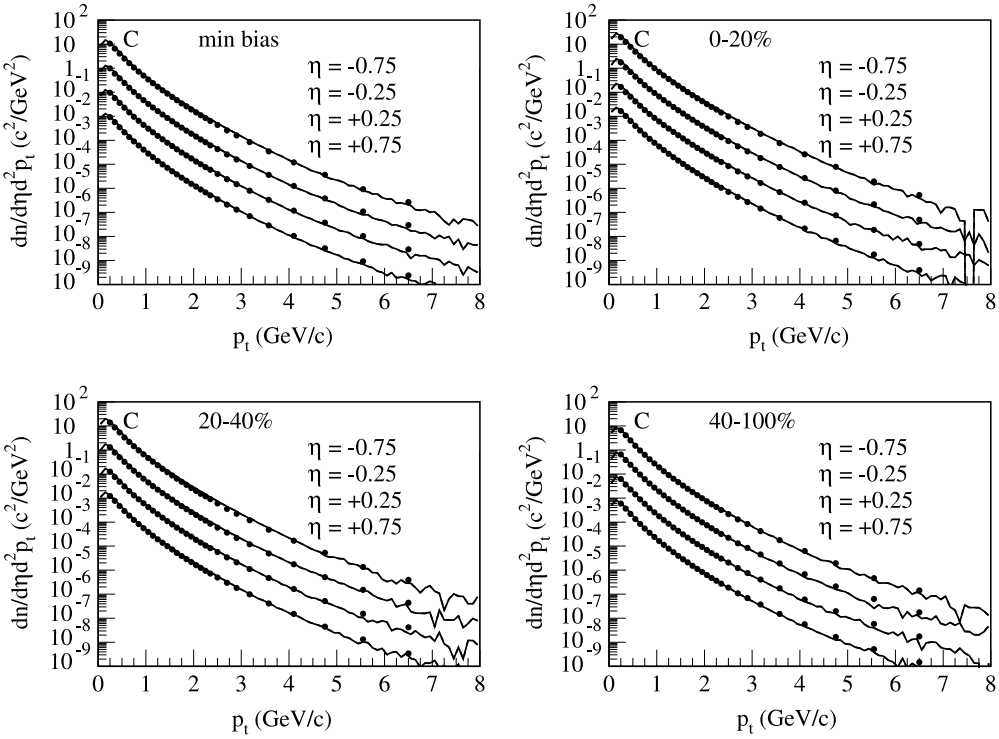

FIG. 18. Transverse momentum spectra of charged particles in dAu collisions at different centralities and at different pseudorapidities. The four figures represent minimum bias, central (0%–20%), midcentral (20%–40%), and peripheral (40%–100%) collisions. For each figure, from top to bottom: $\eta = -0.75$, $\eta = -0.25$, $\eta = 0.25$, $\eta = 0.75$. Lines are EPOS simulations; points are data [4]. Different curves have been displaced by factors of 10.

expect that the pp reference spectrum is 10%–20% too low, which means $R_{d\mathrm{Au}}$ is 10%–20% too high. The corresponding reduction would bring the STAR data down to the EPOS simulation curve (full line), and they would agree with the PHENIX, and the PHOBOS data. BRAHMS is on the lower end, but within the error bars compatible with the simulation curve.

In Fig. 23, we consider charged particle nuclear modification factors in minimum bias dAu collisions at (or close to) $\eta = 1$, together with the corresponding simulations.

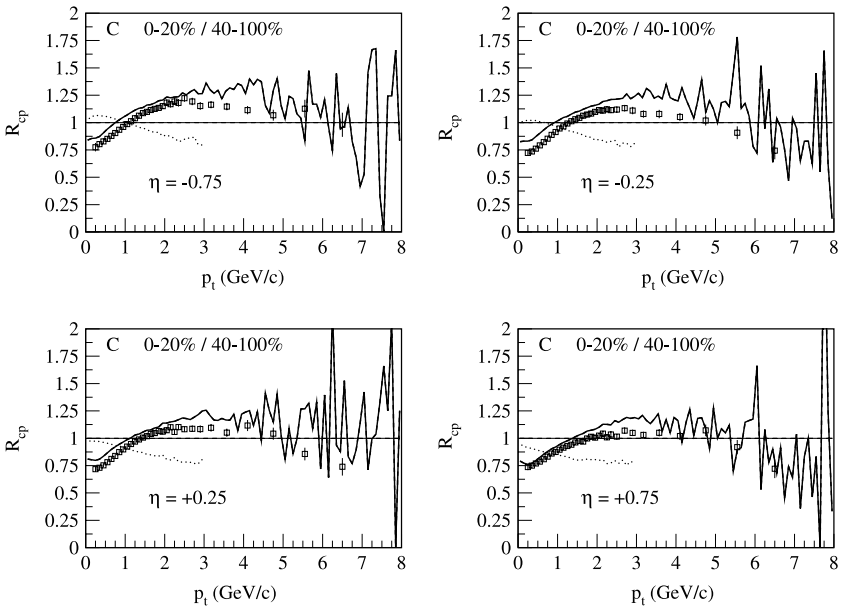

FIG. 19. R_{cp} ratios for charged particles at different pseudorapidities. Solid lines are EPOS simulations; points are data [4]. Dotted lines are EPOS simulations with parton ladder splitting turned off.

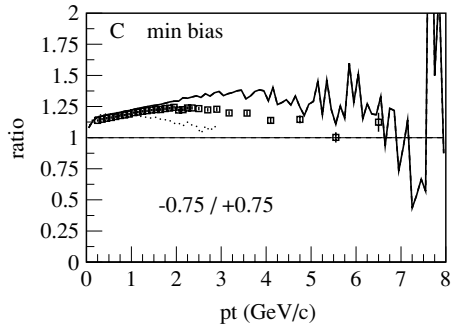

FIG. 20. Ratio of charged particle spectra at backward to forward pseudorapidities ($\eta = -0.75/\eta = 0.75$), in minimum bias dAu collisions. Solid line is EPOS simulation; points are data [4]. Dotted line is EPOS simulation, with parton ladder splitting turned off.

We show minimum bias data at $\eta = 0.8$ from PHOBOS [8] and at $\eta = 1$ from BRAHMS [7]. We also show minimum bias EPOS simulations at $\eta = 1$ and $\eta = 0.8$; they are very close to each other. The data are somewhat lower, but the curves are within the error bars. A systematic difference may again be due to the pp reference. To investigate this, we also plot a "mixed" $R_{d\mathrm{Au}}$: the nuclear spectrum is taken from BRAHMS, but we use the EPOS pp reference. The result (squares) now exceeds the simulation curve.

In Fig. 24, we finally compare EPOS simulations with data from BRAHMS [7] at $\eta = 2.2$ and $\eta = 3.2$. Data and simulations agree quite well.

VII. SUMMARY

In this paper, we presented a phenomenological approach, called EPOS, that is based on the parton model but goes much beyond it by considering elastic and inelastic parton ladder splitting.

The main effect (at least concerning the observables investigated in this paper) is due to the fact that inelastic splitting (bifurcation of parton ladders) leads to a modified hadronization process, a "collective hadronization" of multiple, parallel parton ladders, on the target side, in the case of dAu collisions. This is the equivalent of string fusion, if one uses the language of strings. But contrary to the usual string fusion picture, here we do not have complete ladders that behave collectively, but only the bifurcated ones on the target side.

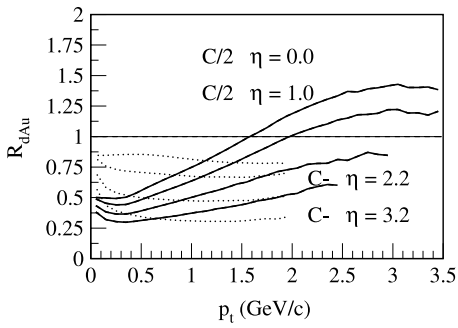

FIG. 21. Nuclear modification factors $R_{d\mathrm{Au}}$ for charged particles (C/2, positive plus negative particles over 2) or negative particles (C-) in minimum bias dAu collisions, at different pseudorapidities. Solid lines are full EPOS simulations; dotted lines are EPOS with parton ladder splitting turned off.

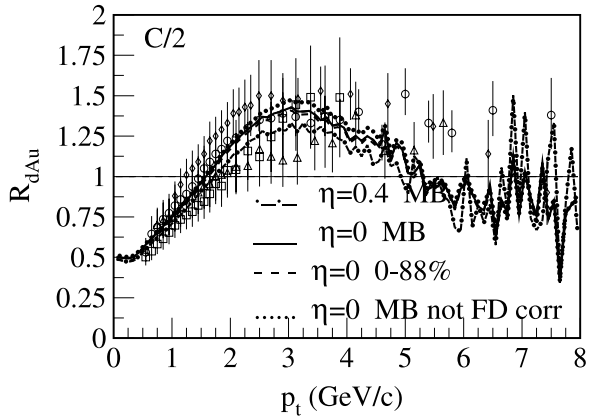

FIG. 22. Nuclear modification factors $R_{d\mathrm{Au}}$ for charged particles in minimum bias dAu collisions at (or close to) $\eta = 0$. Lines are full EPOS simulations: minimum bias at $\eta = 0$ (full), at $\eta = 0.4$ (dashed-dotted), not feed-down corrected (dotted), 0%–88% centrality, at $\eta = 0$ (dashed). Points are minimum bias data at $\eta = 0$ from STAR [5] (rhombs), at $\eta = 0.4$ from PHOBOS [8] (squares), 0%–88% centrality data at $\eta = 0$ from PHENIX [6] (circles), and minimum bias results at $\eta = 0$ from BRAHMS [7] (triangles).

Concerning p_t spectra, the main effect of collective hadronization is a p_t broadening. This is certainly what is needed; but real evidence for our picture can only come from a very detailed comparison with all corresponding data currently available. For this purpose, we considered all published nuclear modification factor data concerning charged particles, from all four RHIC experiments. We investigated in detail

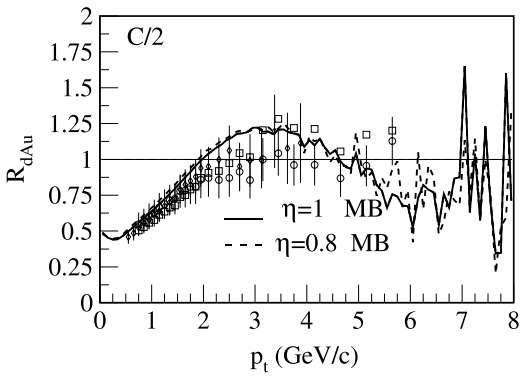

FIG. 23. Nuclear modification factors $R_{d\mathrm{Au}}$ for charged particles in minimum bias dAu collisions at (or close to) $\eta = 1$. Lines are full EPOS simulations: minimum bias at $\eta = 1$ (full), at $\eta = 0.8$ (dashed). Points are minimum bias data at $\eta = 0.8$ from PHOBOS [8] (rhombs), at $\eta = 1$ from BRAHMS [7] (circles). Squares represent $R_{d\mathrm{Au}}$ calculated from the BRAHMS dAu p_t spectrum and the pp simulation result.

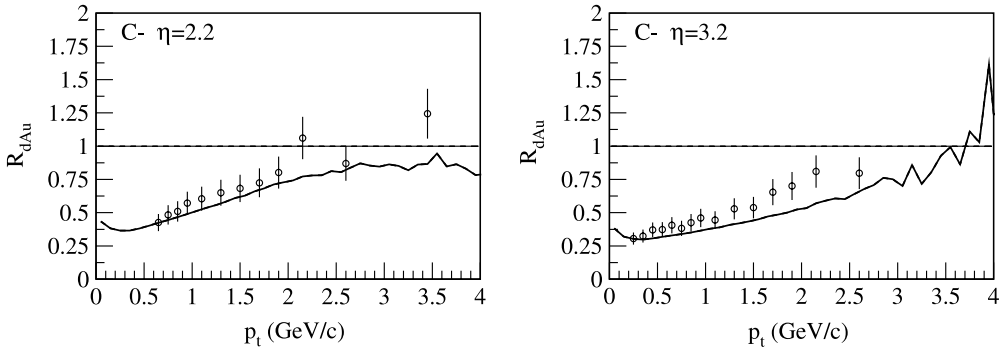

FIG. 24. Nuclear modification factors $R_{d\mathrm{Au}}$ for negative particles in minimum bias dAu collisions at $\eta = 2.2$ (left) and $\eta = 3.2$ (right). Lines are full EPOS simulations; points are data from BRAHMS [7].

the rapidity dependence of nuclear effects, and we found a slightly decreasing broadening with increasing pseudorapidity, in perfect agreement with the data.

ACKNOWLEDGEMENT

F.M.L. acknowledges the support of the National Natural Science Foundation of China (NSFC-10505010).

[1] J. Adams *et al*. (STAR Collaboration), Phys. Rev. Lett. **91**, 172302 (2003).
[2] S. S. Adler *et al*. (PHENIX Collaboration), Phys. Rev. C **69**, 034910 (2004).
[3] S. S. Adler *et al*. (PHENIX Collaboration), Phys. Rev. C **69**, 034909 (2004).
[4] J. Adams *et al*. (STAR Collaboration), Phys. Rev. C **70**, 064907 (2004).
[5] J. Adams *et al*. (STAR Collaboration), Phys. Rev. Lett. **91**, 072304 (2003).
[6] S. S. Adler *et al*. (PHENIX Collaboration), Phys. Rev. Lett. **91**, 072303 (2003).
[7] I. Arsene *et al*. (BRAHMS Collaboration), Phys. Rev. Lett. **93**, 242303 (2004).
[8] B. B. Back *et al*. (PHOBOS Collaboration), Phys. Rev. C **70**, 061901 (2004).
[9] D. Kharzeev, E. Levin, and L. McLerran, Nucl. Phys. **A748**, 627 (2005); D. Kharzeev, Y. V. Kovchegov, and K. Tuchin, Phys. Rev. D **68**, 094013 (2003).
[10] R. Baier, A. Kovner, and U. A. Wiedemann, Phys. Rev. D **68**, 054009 (2003).
[11] J. L. Albacete, N. Armesto, A. Kovner, C. A. Salgado, and U. A. Wiedemann, Phys. Rev. Lett. **92**, 082001 (2004).
[12] J. Jalilian-Marian, Y. Nara, and R. Venugopalan, Phys. Lett. **B577**, 54 (2003); A. Dumitru and J. Jalilian-Marian, Phys. Rev. Lett. **89**, 022301 (2002).
[13] R. C. Hwa and C. B. Yang, Phys. Rev. C **70**, 037901 (2004); **70**, 054902 (2004).
[14] X.-N.-Wang, Phys. Lett. **B565**, 116 (2003).
[15] I.-Vitev, Phys. Lett. **B562**, 36 (2003).
[16] A. Accardi and M. Gyulassy, Phys. Lett. **B586**, 244 (2004).
[17] Z. W. Lin and C. M. Ko, Phys. Rev. C **68**, 054904 (2003).
[18] H. J. Drescher, M. Hladik, S. Ostapchenko, T. Pierog, and K. Werner, Phys. Rep. **350**, 93 (2001).
[19] M. Bleicher, F. M. Liu, A. Keränen, J. Aichelin, S. A. Bass, F. Becattini, K. Redlich, and K. Werner, Phys. Rev. Lett. **88**, 202501 (2002).
[20] F. M. Liu, J. Aichelin, M. Bleicher, H. J. Drescher, S. Ostapchenko, T. Pierog, and K. Werner, Phys. Rev. D **67**, 034011 (2003).
[21] J. Adams *et al*. (STAR Collaboration), Phys. Lett. **B616**, 8 (2005).
[22] C. Caso *et al*., Eur. Phys. J. C **3**, 1 (1998).
[23] G. Giacomelli and M. Jacob, Phys. Rep. **55**, 1 (1979).
[24] G. J. Alner *et al*., Z. Phys. C **33**, 1 (1986).
[25] F. Abe *et al*., Phys. Rev. D **41**, 2330 (1990).
[26] G. J. Alner *et al*. (UA5 Collaboration), Z. Phys. C **33**, 1 (1986).
[27] J. Adams *et al*. (STAR Collaboration), Phys. Rev. Lett. **91**, 172302 (2003).
[28] PHENIX Collaboration, Phys. Rev. Lett. **91**, 241803.
[29] B. B. Back (PHOBOS Collaboration), Phys. Rev. Lett. **93**, 082301 (2004).
[30] BRAHMS Collaboration, Phys. Rev. Lett. **94**, 032301 (2005).
[31] PHOBOS Collaboration, Phys. Rev. C **72**, 031901 (2005).